Delft University of Technology

Post peel test assessment of metal-metal bonded interface using hyperspectral imaging

Papadakis, Vassilis; Teixeira De Freitas, Sofia; Colijn, Rogier; Goedhart, Jonne; Poulis, Hans; Groves, Roger

Post peel test assessment of metal-metal bonded interface using hyperspectral imaging

V. M. Papadakis[1], S. Teixeira de Freitas[2], R. M. Colijn[1], J. J. Goedhart[1], J. A. Poulis[2], R. M. Groves[1]
[1]Aerospace Non-Destructive Testing Laboratory, Delft University of Technology
[2]Structural Integrity & Composites, Delft University of Technology
Kluyverweg 1, 2629 HS Delft, The Netherlands

ABSTRACT

The adhesion process of bonded structures is a very sensitive manufacturing process, namely to surface contaminations. Nowadays, the adhesion quality of bonded joints can only be detected by destructive testing such as peel tests. But, for actual structures destructive testing of every bonded part is obviously not an option and industry is lacking a non-destructive test to quantify adhesion strength. In this work a methodology is described that could lead to a successful detection of possible contamination agents during the manufacturing process of bonded structures. Hyperspectral imaging is an optical non-destructive technique that allows mapping of specific chemical characteristics of a surface in high contrast. It is a well-recognized technique that has already been successfully applied in a wide range of fields including astronomy, remote sensing, cultural heritage and medical sciences.

Multiple sets of aged and non-aged peel tests were destructively tested under different conditions. One type of adhesively bonded specimens was studied: aluminium-to-aluminium using standard floating roller peel test (ASTM D3167). Five sets of samples with different aging conditions were tested. After destructive testing, the contamination level of the fracture surfaces of the bonded specimens were studied using hyperspectral imaging. The hyperspectral imaging system used was a line-scan spectral imaging device (Imspector V10E spectrograph, SPECIM, Finland) capable of acquiring data in the range of 400 nm – 1000 nm with a bandwidth of 2.8 nm. Three tungsten halogen light sources (30W, Osram) were used for uniform illumination across all the sensitivity range of the sensor. The resulting images of each specimen had a resolution of 1312 * 300 pixels, with an exposure time of 200 msec. Following acquisition, all measurements were normalized with the use of a white diffuse reference target (WS1, Ocean Optics). Reference reflectance spectra were extracted from suspicious areas and a non-negative-least-square un-mixing algorithm was applied to check for chemical similarities. Two main signals were detected and mapped onto the surfaces. Statistical analysis was performed, based on the mapping results that described the surface percentage coverage of the contaminant signals and the related statistical errors. A correlation between the percentage of contamination and the adhesive failure was found. Results are promising and will be further studied with other techniques and chemical analyses to fully understand the level of contamination.

Keywords: composites, adhesive bond, non-destructive testing, aerospace, optical diagnosis, hyperspectral imaging

*V.Papadakis@tudelft.nl; phone: +31 15 27 82795; aerondt.tudelft.nl

1. INTRODUCTION

Adhesive bonding is a very promising joining technology in terms of weight and performance for assembling structural parts as an alternative to mechanical fasteners. However, the adhesion process is a very sensitive manufacturing process, namely to surface contaminations. It has been used as a joining technology for structural applications for several decades in automotive industry, aerospace industry, wind energy, etc. It is well known that in order to guarantee a good performance of bonded structures, interfacial failure must be avoided. This can only be achieved if a good interface adhesion between the adhesive and the adherends is guaranteed. Nowadays, interface adhesion quality of bonded joints can only be detected by destructive testing such as peel tests. For metal bonding, a widely accepted industrial test to

assess the interfacial adhesion is the standard floating roller peel test [1]. A cohesive failure in either the adhesive or adherend when peeling-off the flexible adherend indicates a good adhesion quality at the interface. This is a fast and reliable destructive test to assess metal bonding adhesion. Research has been performed using these types of peel tests for several purposes, including the screening of adhesives and surface pre-treatments [2-6].

However, up to now, industry is lacking a non-destructive test (NDT) to assess and quantify adhesion strength. The nonexistence of such an NDT is the main reason for the lack of acceptance of adhesive bonding in aircraft structures. Currently, bonded joints are only allowed in primary aircraft structures if the ultimate load is guaranteed by other design features in case total disbond occurs [6]. These design features are the so called *chicken rivets*. This certification rule results current bonded joints in primary aircraft structure are being reinforced with rivets for certification purposes. These hybrid bonded joints (adhesive bond + riveting) are inefficient, in terms of performance-to-weight ratio when joining composite parts. There are only a few techniques that have the advantages of being non-destructive, optical and able to characterize surface chemical differences remotely such as XRF, FORS, etc. Hyperspectral imaging is such a technique, based on the combination of imaging and spectroscopy, that enables the mapping of specific chemical characteristics of a surface in high contrast. It is a well-known technique that is rapidly evolving and has already been successfully applied in a wide range of fields including astronomy, remote sensing [7], coatings [8], food quality [9, 10], engineering [11], cultural heritage [12-14] and medical sciences [15, 16].

In this work we describe a methodology based on hyperspectral imaging, in the visible and near infrared regions (400 nm – 1000 nm) used to characterize the chemical composition of materials that can lead to a successful detection of possible contamination agents during the manufacturing process.

2. DESTRUCTIVE TESTS: SPECIMENS AND TEST SETUP

Standard floating roller peel tests were performed using the epoxy film adhesive AF163-2 (3M, Maplewood, Minnesota, USA) at five different tests conditions. This is an adhesive commonly used for aerospace manufacturing and is a representative adhesive for testing.

2.1 Materials and Specimens

The peel specimens are based on the ASTM standard D3167 [1]. A 1.6 mm thick aluminium sheet (rigid adherend) was adhesively bonded to a 0.5 mm thick aluminium sheet (flexible adherend). During testing, the flexible adherend was peeled off from the rigid adherend. Both aluminium adherends were clad aluminium alloy 2024. Prior to bonding, the aluminium surfaces were pre-treated with chromic acid anodizing and primed with BR 127 (Cytec Engineered Materials, Tempe, Arizona, USA). The specimens were cured in the autoclave according to the adhesive manufacturer's recommendation for 60 minutes at 120°C, under 3 bar pressure. The bonded panels were 100 mm wide by 300 mm long. After the curing process, the panels were water jet cut into 25 mm wide specimens. Figure 1 shows a drawing of the test panels. The final adhesive thickness was determined by subtracting, the thicknesses of the adherend from the total thickness. The one standard deviation bondline thickness was 0.26 ± 0.06 mm.
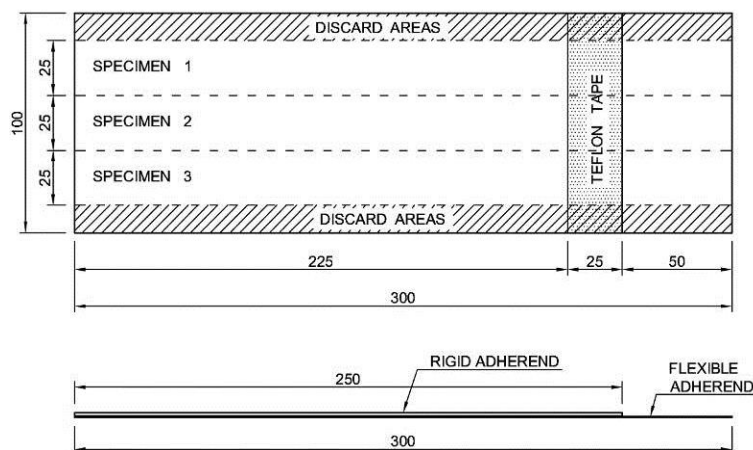

Figure 1. Bonded test panel (dimensions in mm) [3].

2.2 Experimental procedure

The experimental procedure of the floating roller peel tests was based on the ASTM standard D3167 [1]. The tests were carried out using an electromagnetic Zwick machine with maximum load capacity of 20 kN, coupled with a load cell of 1 kN. Tests were carried out at displacement controlled with a testing speed of 125 mm/min. Figure 2 shows the peel test setup. During tests, the load and the cross head displacement were recorded.

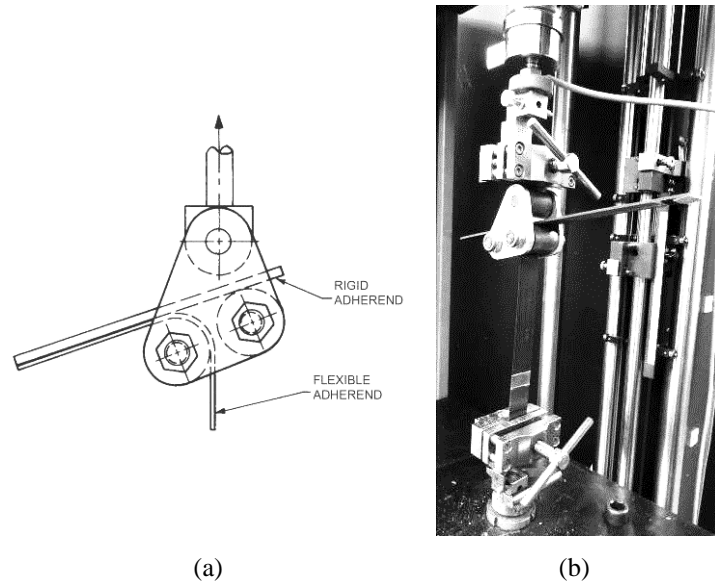(a)   (b)

Figure 2. Peel test setup: (a) schematic diagram of the floating roller [1], (b) photograph of the peel test in action [3].

The samples were exposed to four different pre-test ageing conditions, then tested at two different temperatures as shown in Table 1. Ageing was performed in a salt-spray and in a climate chamber. Testing was performed in a heated peel testing machine. In order to test at different temperatures, a climate chamber was coupled to the testing machine. A total of three specimens were tested in each test condition.

Table 1. Peel test conditions.

Test Series	Aging conditions	Temperature during testing	# of specimens
(1)	None	Room Temperature (RT)	3
(2)	None	+80°C	3
(3)	30 days at the Salt Spray (SS) cabinet	RT	3
(4)	15 days at 75°C and 85% Relative Humidity (RH)	RT	3
(5)	30 days at 75°C and 85% RH	RT	3

3. HYPERSPECTRAL IMAGING

Hyperspectral imaging (HSI) measurements were performed in the visible and near infrared region (400 nm – 1000 nm) to study the absorption characteristics of the specimen fracture surfaces. This wavelength region is commonly used in analytical chemistry for the quantitative determination of organic compounds.

3.1 The HSI setup

The experimental setup used is an imaging monochromator IMSPECTOR V10E (Specim©), with a spatial resolution of 1312 pixels operating in the wavelength range of 400 - 1000 nm, with a bandwidth of 2.8 nm. This setup is located in the Aerospace Non-Destructive Testing Laboratory at TU Delft and is equipped with an automated scanning platform for measuring specimens up to a size of 21 by 40 cm as shown in Figure 3. Scanning occurs on the large side of the platform, with speeds as low as 0.1 mm/sec. An objective lens (Xenoplan, Schneider) with a focal length of 35 mm was used to image the specimen from a distance of 15 cm, resulting to a 3 cm of field of view. A flattening filter (Specim©) was used, coupled in front of the objective lens, to reduce the sensitivity in the middle of the spectrum, allowing the relative enhancement of the sensor sensitivity close to its limits range (UV and IR part of the spectrum).
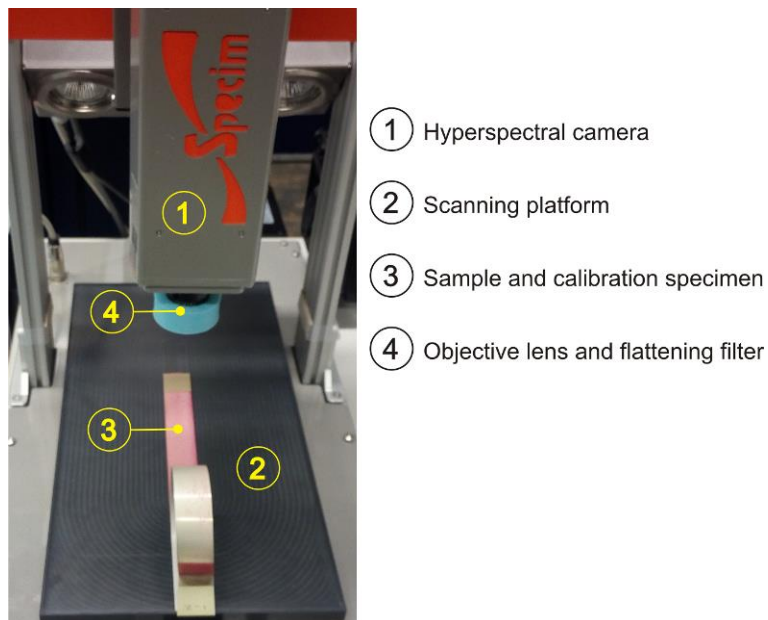

Figure 3. Photo of the laboratory hyperspectral imaging setup.

Specimens were illuminated by 3 tungsten light sources (30W Halogen, OSRAM), provided by the manufacturer, with a 45 degree angle of incidence in respect to the sample and the sensor to avoid any possible specular reflections reaching the monochromator. In such a geometry, the sensor was recording only the diffuse scattering light caused by the surface roughness and scattering centers underneath the surface. The control of the basic parameters of the sensor (frame rate [fps], exposure time [ms], spectral and spatial binning) and scanner (scanning speed [mm/sec], total scanning distance [mm]) was achieved through SpectralDAQ solution software© (Specim).

3.2 Calibration

The measurements were calibrated by the use of a Diffuse Reflectance Target (DRT) made out of spectralon (WS1, Ocean Optics). DRT measurements were achieved by acquisition of 100 lines from the WS1 without moving the scanner. These line scans were averaged to produce the calibration reference vector. The calibration reference vector was further corrected by the reference reflectivity curve as provided by the manufacturer to achieve a flat reflectivity line. Acquisition of the DRT data was performed after each measurement without changing the experimental conditions. Dark noise measurements were achieved similarly as the DRT data, with the sensor electronic shutter closed and by keeping the shutter value constant. Through averaging of 100 lines the dark noise reference vector was calculated.

Specimen and DRT images were first corrected for dark noise by subtracting the dark noise reference vector from each line-scan data. Normalization of the specimen images was achieved by dividing each line scan measurement with the relative calibration reference vector. Normalization assisted in correcting various parameters including: the spectral reflectance curves, the interference noise coming from the SPECIM optics, any possible dust in the optics, and the illumination light inhomogeneities.

3.3 Measurements and Analysis

Acquisition of HSI images was performed by scanning one specimen each time. The image resolution on the scanning direction was selected to be 300 lines. The sensor's exposure time was set to 200 msec with a framerate of 3.5 fps, while the scanning speed of the platform was set to 0.2 mm/sec. With the above settings each measurement had a total acquisition time of 86 seconds, an image size of 3.0 by 1.7 cm, and a signal close to 80% of the maximum of the sensor dynamic range.

Analysis of the HSI data was performed using the new software analysis platform (TIPP, TU Delft), developed in the Aerospace Non-Destructive Testing Laboratory at the Delft University of Technology [17]. The specimens were initially normalized (with white reference and dark noise removed), then processed (cropped) to reduce the amount of data for analysis. Following this they were visually inspected and reference spectra were extracted from the areas of interest. There were three reference areas selected: (1) "pure" adhesive (adhesive A), this was done by selecting the most clean spots on the image and averaging; (2) bright spots on the specimens (adhesive B); (3) dark contaminated spots on the specimen (contamination A). Reference Component Analysis (RCA) involved processing of the selected separate reference vectors in combination with the standard Non-Negative Least Squares un-mixing algorithm (NNLS) [18]. NNLS un-mixing algorithm was used to estimate the set of distinct reference vectors that constitute each mixed pixel, resulting in weight maps for each reference vector. These weights were then visualized in colored heat maps showing the identified locations and the surface percentage covering of the reference vectors (i.e. contamination agent) present. In the Figure 4 a screenshot of the RCA visualization module is displayed showing how the NNLS RCA module in the platform displays data to the user.
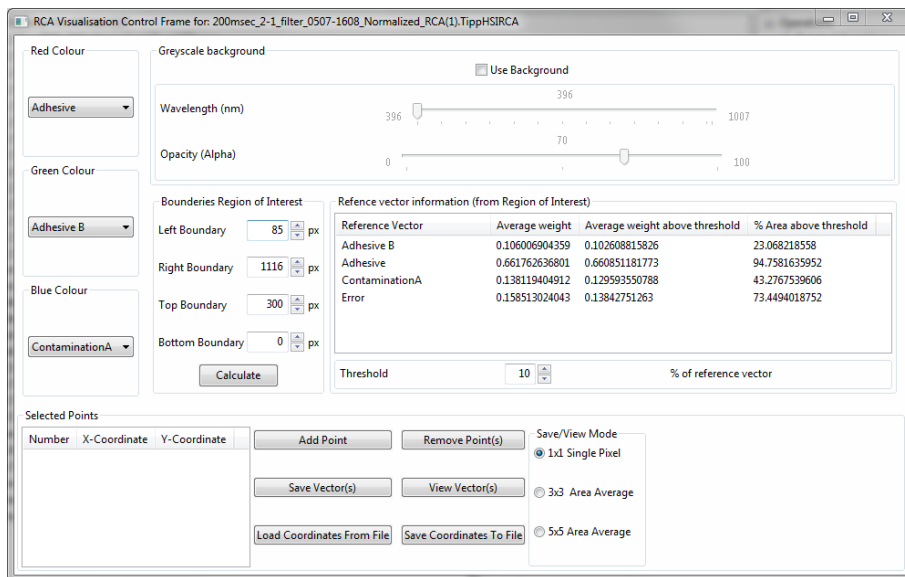

Figure 4. Screenshot from the TU Delft Image Processing Platform depicting the RCA visualization module

In order to determine the rate of the contribution of a certain reference vector in the specimens' surface area a threshold value is introduced for error control. This threshold value defines the percentage of erroneous level accepted in the calculation. It describes the minimum percentage of a reference vector contribution in a pixel to include it in the *affected* area calculation. Applying this threshold value across the array and averaging the weights that are greater than the threshold it is possible to determine a rate of contamination in the specimens' surface.

4. EXPERIMENTAL RESULTS

4.1 Peel test results

Figure 5 shows the typical load displacement curves measured during peel test for each test series. The average peel strength was determined along 150 mm of displacement, disregarding the first 15 mm after a first peak (decrease of about 5%). This procedure for determining peel strength values follows the procedure described in section 2.2.
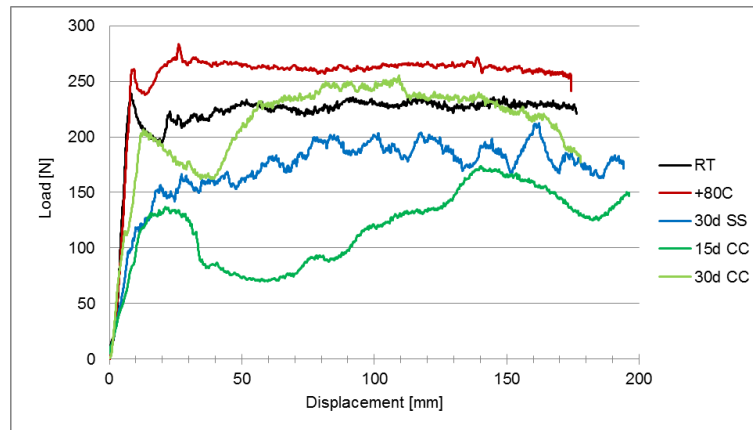

Figure 5. Characteristic load displacement curves from one sample of each of the five series of peel tests.

Table 2 gives the average peel strength values and the average % of failure mechanism observed on the specimens tested. Two types of failure mechanisms were observed: cohesive failure (CF) and adhesive failure (AF). AF indicates a bad adhesion between the adhesive and the adherend, since the failure occurs at the interface. CF indicates good adhesion, since the failure occurs inside the adhesive layer and not at the interface.

The % of failure mode indicated in Table 2 was based on an area estimation of each failure mode by visual observation of the specimens' fracture surface after testing. The % of failure mode are therefore rough estimations with an error of ±10%.

Table 2. Peel test results (F peel - average peel strength and percentage of cohesive failure (CF) and adhesive failure (AF)), determined visually.

Test series	F peel	Failure mode	
	(N/ 25 mm)	CF	AF
(1) RT, no aging	222	90%	10%
(2) +80°C, no aging	265	100%	0%
(3) RT, 30 days SS	161	80%	20%
(4) RT, 15 days 75°C 85%RH	102	33%	67%
(5) RT, 30 days 75°C 85% RH	191	83%	17%

4.2 Spectral Imaging Results

The first 17 mm of the fracture surface of each peel specimens was analyzed using hyperspectral imaging. In Figure 6 the reference vectors from the identified areas are presented. These points come from an average of 5 reference vectors from similar points across the specimen surface. It can be seen that for the adhesive A and adhesive B vectors, the main differences appear in the regions between 400 and 500 nm, as also for a small offset difference in the region between 600 and 1000 nm. The contamination A vector shows strong differences across all the wavelength sensitivity range, with a slightly increased absorption at 850 nm with a bandwidth of approximately 200 nm.
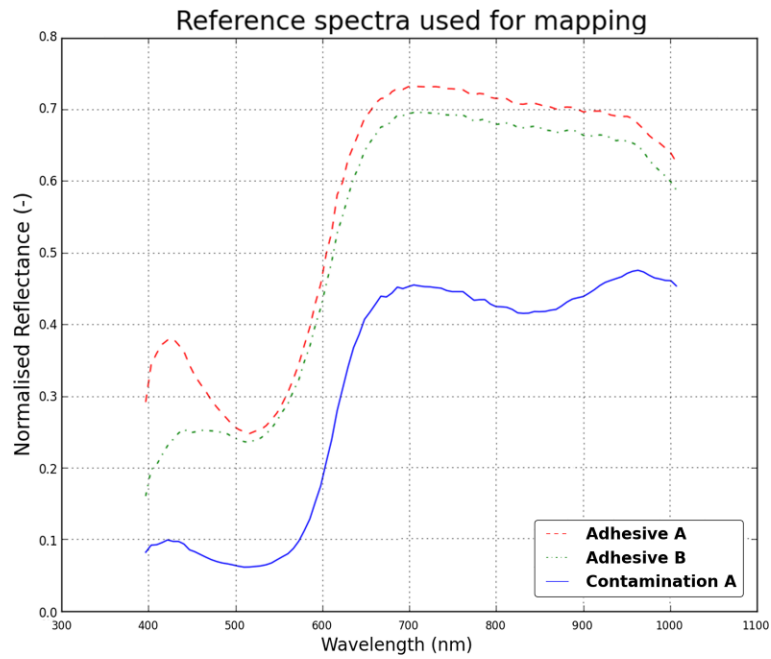
Figure 6. Reference reflection curves from the selected surface areas

The reflection curve of adhesive A comes a fracture surface with cohesive failure. Adhesive B curve refers to a fracture surface with cohesive failure but with an increased reflectivity (whitening effect). Contamination A curve shows the reflectance from the most visually defined contamination area. The contamination area identified was further supported by the fact from the adhesive remains on the opposite aluminium surface of the bond.

The results of the non-negative least squares un-mixing algorithm for one of the high temperature 80°C non-aged samples can be seen in Figure 7 with specimen 2 shown as an example. Figure 7a is the sample viewed using R, G, B colors. Figure 7b is the pseudo-color map of the three reference vectors and Figure 7c is the error map calculated by the NNLS un-mixing algorithm.
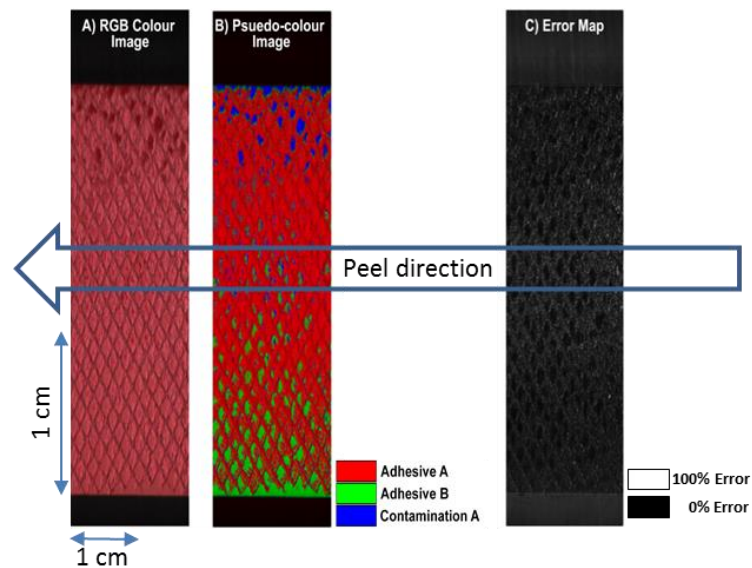

Figure 7. RCA images of specimen 2: (a) R, G, B color image, (b) Pseudo-color image (c) Error map

In specimen 2 the average error calculated is equal to 14.9%. The percentage of surface vector contribution, when a threshold of 10.0% is considered, is equal to 94.8% for adhesive A, 23.0% for adhesive B and 43.3% for contamination A.

Results of five typical specimens are shown in Figure 8 using the same pseudo-color heat maps. From left to right the specimens presented are: (1) non-aged specimen tested at room temperature (RT), (2) non-aged specimen tested in high temperature +80°C (HT), (3) aged specimen for 30 days in the salt spray cabinet tested in RT, (4) aged specimen for 15 days at 75°C and 85% relative humidity tested at RT, and (5) aged specimen for 30 days at 75°C and 85% relative humidity tested at RT. In specimen 3 it can be seen that a severe corrosion of the surface has occurred in two areas.
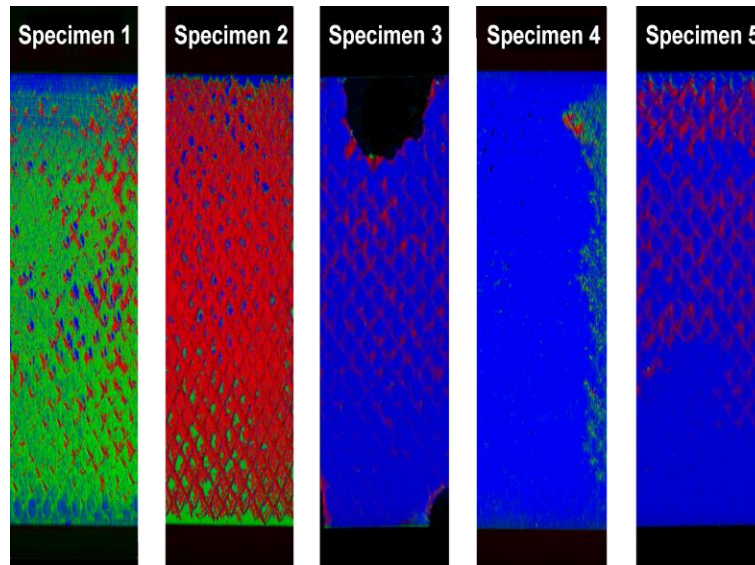

Figure 8. RCA resulting pseudo-color images from 5 peel test specimens subjected to different environmental conditions.

The percentages of the contamination level as determined using RCA are shown in Table 3. As seen, specimen 2 has 13% of contamination in the surface, which is assumed to be a standard contamination level.

Table 3. Contamination percentage in each specimen type.

	specimen 1	specimen 2	specimen 3	specimen 4	specimen 5
Adhesive Failure %	10	0	20	67	17
Contamination %	25	13	33	67	35

In the following Figure 9 the percentages of the area of adhesive failure and the contamination are shown for comparison purposes.
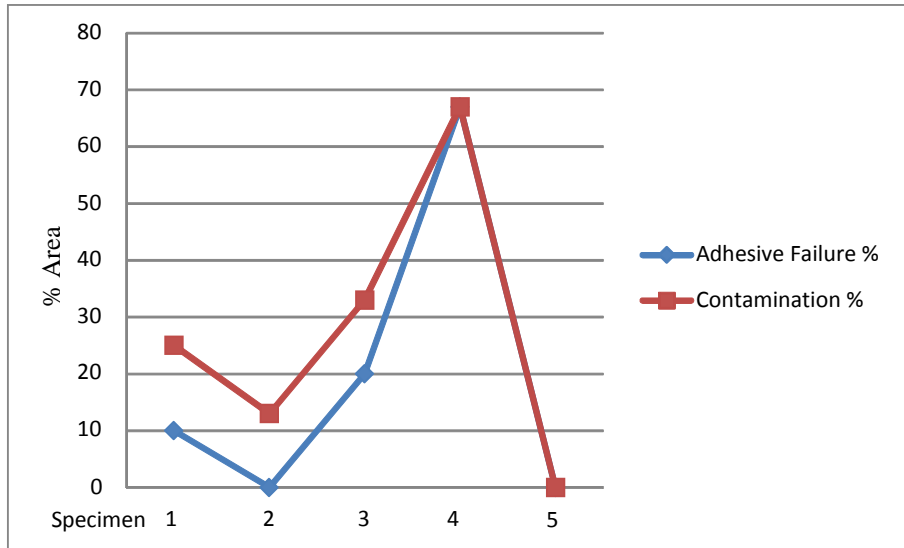
Figure 9: Percentage of the area of adhesive failure and contamination of the 5 specimens tested.

Comparing the values per specimen in Table 3 and Figure 9, one can see that there is a strong correlation between the contamination percent after correction with the adhesive failure values for each specimen type.

5. DISCUSSION

In this paper the monitoring of contaminant agents on metallic surfaces has been demonstrated. The results deriving from hyperspectral imaging are promising as they show that it is possible to map, in high contrast, the reference components across the surfaces of the samples. Further, the results of RCA provide the contribution percentages on the specimen surface for each reference vector. These results together with the error calculation assist in understanding of the strength test result variations. The specimen types showed different amounts of weight percentages which were used to compare against relative strength tests.

Adhesive B points identified refer to a specific effect of change of the polymer structure, which exhibits a change in color after it has been severely stressed under a load. Under stress the polymer chains will straighten, slip and shear within the plastic's microenvironment. Occlusions or holes are formed by the movement of fillers and the polymer chains. These clustered occlusions form micro-voids. When these micro-voids obtain a size greater than or equal to the wavelength of light (380 - 750 nm), the light is scattered and the object appears white (stress whitening). The micro-voids thus change the refractive index of the plastic.

The non-negative-least-squares un-mixing algorithm is an iterative process that finds the best solution to the equation $Ax = b$, where A is the matrix consisting of the reference vectors and b is the specimen vector. The result of this process will not be exact, thus there will always be a residual, equal to $Ax - b$. This residual is the error analysis that is also mapped for each specimen to provide an understanding of possible variations of the contamination percentage results with the strength peel tests.

Lastly, it should be noted that the sample area inspected with the hyperspectral imaging method was 17 mm, while the peel strength test results presented in Figure 5 refer to 150 mm peel length. To further correlate the two methods across the full peel length in each specimen, further tests are required.

6. CONCLUSIONS

Fifteen adhesively bonded surfaces have been aged at five different environmental conditions. Specimens were then peel tested for strength. After testing, their surfaces were analysed using a hyperspectral imaging setup that allowed for high contrast mapping of contamination under selected reference vectors. Along with this mapping it was also possible to determine the percentage of contamination on the surface. Comparing the hyperspectral imaging results with the strength test results a strong correlation was found.

ACKNOWLEDGMENTS

REFERENCES

[1] ASTM Standard D3167-10, "Standard Test Method for Floating Roller Peel Resistance of Adhesives", ASTM International, www.astm.org (2010).

[2] Bishopp, J. A., Sim, E. K., Thompson, G. E., and Wood, G. C., "The Adhesively Bonded Aluminum Joint - the Effect of Pretreatment on Durability," Journal of Adhesion, 26(2-3), 237-263 (1988).

[3] de Freitas, S. T., and Sinke , J., "Test method to assess interface adhesion in composite bonding," Applied Adhesion Science, 3(9), (2015).

[4] Hart-Smith, L. J., "A peel-type durability test coupon to assess interfaces in bonded, co-bonded, and co-cured composite structures," International Journal of Adhesion and Adhesives, 19(2-3), 181-191 (1999).

[5] Sargent, J. P., "Durability studies for aerospace applications using peel and wedge tests," International Journal of Adhesion and Adhesives, 25(3), 247-256 (2005).

[6] de Freitas, S. T., and Sinke, J., "Adhesion Properties of Bonded Composite-to-Aluminium Joints Using Peel Tests," Journal of Adhesion, 90(5-6), 511-525 (2014).

[7] Goetz, A. F. H., "Three decades of hyperspectral remote sensing of the Earth: A personal view," Remote Sensing of Environment, 113, Supplement 1, S5-S16 (2009).

[8] Dingemans, L. M., Papadakis, V. M., Liu, P., Adam, A. J. L., and Groves, R. M., "Optical coherence tomography complemented by hyperspectral imaging for the study of protective wood coatings," Optics for Arts, Architecture, and Archaeology V, 9527, (2015).

[9] Gowen, A. A., O'Donnell, C. P., Cullen, P. J., Downey, G., and Frias, J. M., "Hyperspectral imaging – an emerging process analytical tool for food quality and safety control," Trends in Food Science & Technology, 18(12), 590-598 (2007).

[10] He, H.-J., and Sun, D.-W., "Hyperspectral imaging technology for rapid detection of various microbial contaminants in agricultural and food products," Trends in Food Science & Technology, 46(1), 99-109 (2015).

[11] Papadakis, V. M., Muller, B., Hagenbeek, M., Sinke, J., and Groves, R. M., "Monitoring chemical degradation of thermally cycled glass-fibre composites using hyperspectral imaging," Proc. SPIE, 9804-28 (2016).

[12] Papadakis, V., Loukaiti, A., and Pouli, P., "A spectral imaging methodology for determining on-line the optimum cleaning level of stonework," Journal of Cultural Heritage, 11(3), 325-328 (2010).

[13] Balas, C., Papadakis, V., Papadakis, N., Papadakis, A., Vazgiouraki, E., and Themelis, G., "A novel hyper-spectral imaging apparatus for the non-destructive analysis of objects of artistic and historic value," Journal of Cultural Heritage, 4, 330s-337s (2003).

[14] Melessanaki, K., Papadakis, V., Balas, C., and Anglos, D., "Laser induced breakdown spectroscopy and hyper-spectral imaging analysis of pigments on an illuminated manuscript," Spectrochimica Acta Part B-Atomic Spectroscopy, 56(12), 2337-2346 (2001).

[15] Vazgiouraki, E., Papadakis, V. M., Efstathopoulos, P., Lazaridis, I., Charalampopoulos, I., Fotakis, C., and Gravanis, A., "A spectral imaging method depicts neuronal myelin loss, without tissue labelling," Microsopy, Published online, (2015).

[16] Papadakis, V., Karavellas, M. P., Tsilimbaris, M. K., Balas, C., and Pallikaris, I. G., "A hyper spectral imaging FUndus camera for the detection and characterization of retinal lesions," Investigative Ophthalmology & Visual Science, 43, U1259-U1259 (2002).

[17] Papadakis, V., [TU Delft Image Processing Platform] TU Delft, TU Delft(2016).

[18] Keshava, N., and Mustard, J. F., "Spectral unmixing," IEEE Signal Processing Magazine, 19(1), 44-57 (2002).